Electric Power Systems Research 199 (2021) 107462

Contents lists available at ScienceDirect

Electric Power Systems Research

journal homepage: www.elsevier.com/locate/epsr

An optimisation model based approach for power systems voltage stability and harmonic analysis

Mariana O.N. Teixeira *, Igor D. Melo, João A.P. Filho

Federal University of Juiz de Fora, Juiz de Fora, Brazil

ARTICLE INFO

Keywords:
Harmonic distortion
Power quality
Voltage stability
Power systems

ABSTRACT

This paper presents a novel optimisation problem formulation for power systems voltage stability and harmonic analysis. The purpose is to evaluate the maximum loadability of an electrical power system considering voltage magnitudes, active/reactive powers, total and individual harmonic distortion limits as inequality constraints. The impact of power quality on the maximum loadability margin is evaluated based on the results of the optimisation problem solved by interior-point method and the proposed indices in which Lagrange multipliers are used to identify sensitive buses of electrical systems due to power quality degradation and voltage instability. Simulations are carried out using IEEE 30-bus power system assuming the insertion of non-linear loads to validate the use of the proposed method and show the applicability of the indices based on Lagrange multipliers for the assessment of both voltage stability and harmonic distortion. Results are compared with the traditional modal analysis to validate the ability of the proposed method for identifying the most critical buses of the system.

1. Introduction

The determination of voltage stability margins represents a continuous challenge for network operators, especially due to the integration of new types of loads such as electric vehicles, battery farms and electronic-based devices according to Aghdam and Khoshkhoo [1] and Rodriguez-Garcia et al. [2]. Additionally, the ever increasing use of non linear loads also represents a huge challenge to the power systems operation. The degradation of power quality is one of the main consequences of the usage of such loads which might be considered for analysing the impact on the power systems operation and planning according to de Melo et al. [3], Tian et al. [4], Bhattacharyya et al. [5].

The development of adequate techniques is necessary to estimate the proximity of an operating point to a voltage collapse and also to understand the mechanism that contributes to an unstable condition, as discussed in [6] and [7].

Static techniques, based on power flow solution, are often used for voltage stability assessment, including the traditional continuation power flow method, developed by Ajjarapu and Christy [8], which can be used to detect critical areas subject to voltage instability. Based on this technique, the maximum loadability and the voltage stability margin of the system can be determined by assuming progressive increments on the scheduled power consumption of load buses. The consequent decreasing behaviour of voltage magnitudes due to increasing power demand can be assessed by the known PV (active power-voltage) curve. According to Overbye et al. [9], QV (reactive power-voltage) curves can also be applied to analyse voltage stability, being useful for determining the size of capacitor banks, static var compensators and other equipments that provide reactive power support as also described by Sharma et al. [10]. Another useful technique is the modal analysis, proposed by Gao et al. [11], in which the eigenvalues and eigenvectors of the Jacobian matrix of the power flow solution is used to determine critical buses of the system, calculating their participation factors to the instability phenomena. Optimal power flow can also be applied for assessing voltage stability as described by Rodriguez-Garcia et al. [2], Salgado and Zeitune [12], Hong and Gau [13].

In the last years, voltage stability indices (VSI) have been widely applied to voltage stability assessment according to Modarresi et al. [14]. The purpose is to measure the proximity of an operating point to an unstable situation. Currently, due to the use of synchronised phasor measurement units (PMUs), these indices can be estimated in real time, as presented by Amador et al. [15] and Dasgupta et al. [16]. Reference [17] presents a Thevenin equivalent impedance based index for voltage stability analysis. The required information is the system topology, PMUs measurements and operational status of synchronous generators.

Reference [2] presents an optimisation model formulation for

* Corresponding author.
E-mail address: mariana.novais@engenharia.ufjf.br (M.O.N. Teixeira).

https://doi.org/10.1016/j.epsr.2021.107462
Received 26 January 2021; Received in revised form 29 April 2021; Accepted 7 July 2021
Available online 16 July 2021

Nomenclature

Constants

$\theta_k^{h,I}$	injected current angle at bus k for harmonic order h
B_{km}^h	line susceptance from bus k to bus m for harmonic order h
G_{km}^h	line conductance from bus k to bus m for harmonic order h
I_k^h	injected current magnitude at bus k for harmonic order h
$H_{\max}$	maximum harmonic order
n_{eq}	number of equality constraints
n_{ineq}	number of inequality constraints
N_L	total number of load buses
N_g	total number of generators
$P_{g,k}^{1,\min}$ / $P_{g,k}^{1,\max}$	minimum/ maximum active power at a given bus k
$Q_{g,k}^{1,\min}$ / $Q_{g,k}^{1,\max}$	minimum/ maximum reactive power at a given bus k
$THD_k^{I,\max}$	maximum current total harmonic distortion at a given bus k
$THD_k^{v,\max}$	maximum voltage total harmonic distortion at a given bus k
$V_{g,k}^{1,\min}$ / $V_{g,k}^{1,\max}$	minimum/ maximum voltage magnitude at a given bus k
$\mathbf{Y}_{bus}^h$	system harmonic admittance matrix

Indices

d_k^v	proposed index for evaluating voltage magnitude
d_k^{thd}	proposed index for evaluating voltage total harmonic distortion
d_k^q	proposed index for evaluating reactive power support

Variables

δ	Lagrange multiplier associated with equality constraints
λ	loadability factor
μ	barrier parameter
π	Lagrange multiplier associated with inequality constraints
θ_{km}^h	voltage angle difference from bus k to bus m for harmonic order h
$f(\mathbf{x})$	objective function
$g(\mathbf{x})$	equality constraint
$\dot{\mathbf{I}}^h$	system harmonic current phasors vector
IHD_k^I	current individual harmonic distortion at a given bus k
IHD_k^v	voltage individual harmonic distortion at a given bus k
$h(\mathbf{x})$	inequality constraint
L	Lagrangian function
P_k^{calc}	calculated active power at a given bus k
$P_{g,k}^1$	generated active power at a given bus k
$P_{l,k}^1$	demanded active power at a given bus k
Q_k^{calc}	calculated reactive power at a given bus k
$Q_{g,k}^1$	generated reactive power at a given bus k
$Q_{l,k}^1$	demanded reactive power at a given bus k
$\mathbf{s}$	slack variables vector
THD_k^I	current total harmonic distortion at a given bus k
V_k^h	voltage magnitude at bus k for harmonic order h
$\dot{\mathbf{V}}^h$	system harmonic voltage phasors vector
$\mathbf{x}$	state variables vector

Acronyms

PMU	Phasor Measurement Unit
VSI	Voltage Stability Indices
KKT	Karush-Kuhn-Tucker

determining the maximum loadability of a 30-bus power system considering loads represented by voltage dependent models. Then, Lagrange multipliers are used to establish VSI to identify the most critical buses being the method validated by a comparison with modal analysis. State-in-mode participation factors and state-in-mode sensitivities are defined by [7] based on the application of modal analysis to determine critical buses which contributed to an unstable condition. Reference [18] evaluates the impacts in electrical operation networks, particularly on the voltage stability margins, due to the presence of wind generation and its intermittent characteristic. Reference [19] presents the calculation of voltage stability margins values by measuring the hypotenuse under the PV and QV curves with the purpose of identifying critical buses of the system subject to voltage instability. In the work proposed by Xu et al. [20], a probabilistic model for the load margin calculation is presented considering renewable power generation, in which the maximum loadability of the system is determined by an optimisation model formulation considering statistical properties of wind and solar generation systems. Reference [21] presents a novel method based on algebraic manipulation of a linear system of power flow equations for determining load margin due to saddle-node and limit-induced bifurcations, which usually occur with the violation of limits of reactive power generation.

It can be noted from a literature review that papers do not consider the impact of harmonic distortion on voltage stability assessment. However, due to degradation of power quality, power systems may operate disrespecting power quality standards, such as [22–24], which can cause several problems including increasing of temperature in cables and machines, protection relays maltripping, telecommunications conflictions, resonance effects, unavailability of transmission lines and multiple contingencies [3].

The main contribution of this paper is an optimisation model based approach is used for determining the maximum loadability of power systems considering harmonic distortion. Operational and power quality indices limits are treated as inequality constraints incorporated to the optimisation problem. The solution is provided by interior-point method being Lagrange multipliers used to determine stability indices to identify sensitive areas of the network related to undervoltages and harmonic pollution.

This paper is divided into four sections, including this introductory one. The proposed method is described in the second section. In the third one, tests and results are presented. Conclusions are highlighted in the last section.

2. Proposed method

2.1. Optimisation formulation

The maximum loadability is determined by the optimal power flow described in this section. The objective function (1) is subject to equality constraints (2) and (3) related to fundamental frequency power flow equations and (4) representing harmonic load flow, respectively. Inequality constraints from (5) to (11) are also incorporated into the optimisation problem considering operational and power quality indices limits.

$$\max \ \lambda \tag{1}$$

subject to:

$$P_k^{calc} - \left(P_{g,k}^1 - \lambda P_{l,k}^1\right) = 0 \qquad k = 1, \cdots, N_L \tag{2}$$

$$Q_k^{calc} - \left(Q_{g,k}^1 - \lambda Q_{l,k}^1\right) = 0 \qquad k = 1, \cdots, N_L \tag{3}$$

$$\dot{\mathbf{V}}^h = \left[\mathbf{Y}_{bus}^h\right]^{-1} \dot{\mathbf{I}}^h \tag{4}$$

$$V_k^{1,\min} \le V_k^1 \le V_k^{1,\max} \qquad k = 1, \cdots, N_L \tag{5}$$

$$0 \le P_{g,i}^1 \le P_{g,i}^{1,\max} \qquad i = 1, \cdots, N_g \tag{6}$$

$$Q_{g,i}^{1,\min} \le Q_{g,i}^1 \le Q_{g,i}^{1,\max} \qquad i = 1, \cdots, N_g \tag{7}$$

$$0 \le THD_k^v \le THD_k^{v,\max} \qquad k = 1, \cdots, N_L \tag{8}$$

$$0 \le THD_k^I \le THD_k^{I,\max} \qquad k = 1, \cdots, N_L \tag{9}$$

$$0 \le IHD_k^v \le IHD_k^{v,\max} \qquad k = 1, \cdots, N_L \tag{10}$$

$$0 \le IHD_k^I \le IHD_k^{I,\max} \qquad k = 1, \cdots, N_L \tag{11}$$

$$THD_k^v = \frac{\sqrt{\sum_{h\neq 1}^{H_{\max}} \left(V_k^h\right)^2}}{V_k^1} \qquad k = 1, \cdots, N_L \tag{12}$$

$$THD_k^I = \frac{\sqrt{\sum_{h\neq 1}^{H_{\max}} \left(I_k^h\right)^2}}{I_k^1} \qquad k = 1, \cdots, N_L \tag{13}$$

$$IHD_k^v = \frac{V_k^h}{V_k^1} \qquad h = 1, \cdots, H_{\max} \tag{14}$$

$$IHD_k^I = \frac{I_k^h}{I_k^1} \qquad h = 1, \cdots, H_{\max} \tag{15}$$

where:

- λ represents the power system loadability factor assuming an equal increment for all the system load buses;
- N_L is the total number of load bus;
- N_g is the total number of generation bus;
- P_k^{calc} and Q_k^{calc} are active and reactive powers calculated for each bus k of the system as function of state variables;
- $P_{g,k}^1$ and $Q_{g,k}^1$ are scheduled active and reactive power generation at a given bus k;
- $P_{l,k}^1$ and $Q_{l,k}^1$ are scheduled active and reactive power loads at a given bus k;
- $\dot{\mathbf{V}}^h$ and $\dot{\mathbf{I}}^h$ represent the phasor voltage and injected current vectors for harmonic orders h, respectively;
- V_k^1 is the voltage magnitude at fundamental frequency ($h = 1$);
- $V_k^{1,\min}$ and $V_k^{1,\max}$ are the lower and upper bounds of the voltage magnitude, indicated by inequality constraint (5);
- $P_{g,i}^1$ is the active power generated at bus i, and $P_{g,i}^{1,\max}$ is the maximum capacity of the corresponding generator, presented by inequality (6);
- $Q_{g,i}^1$ is the reactive power generated at bus i, $Q_{g,i}^{1,\min}$ and $Q_{g,i}^{1,\max}$ are the minimum and maximum reactive power value, presented by inequality (7);
- THD_k^v and $THD_k^{v,\max}$ are voltage total harmonic distortion and its corresponding maximum value;
- THD_k^I and $THD_k^{I,\max}$ are current total harmonic distortion and its corresponding maximum value;
- IHD_k^v and $IHD_k^{v,\max}$ are voltage individual harmonic distortion and its corresponding maximum value;
- IHD_k^I and $IHD_k^{I,\max}$ are current individual harmonic distortion and its corresponding maximum value;

Voltage THD and IHD are calculated, respectively, by Eqs. (12) and (14) in which $H_{\max}$ represent the maximum harmonic order considered by the study. Current THD and IHD are determined by Eqs. (13) and (15), respectively.

It is important to notice that the fundamental frequency power load flow is represented by traditional Eqs. (2) and (3), which considers the power generation and loading.

The calculated values of fundamental frequency active and reactive powers are determined by (16) and (17), respectively, according to traditional power flow equations.

$$P_k^{calc} = V_k^1 \sum_{m\in K} V_m^1 \left(G_{km}^1 cos\left(\theta_{km}^1\right) + B_{km}^1 sen\left(\theta_{km}^1\right)\right) \tag{16}$$

$$Q_k^{calc} = V_k^1 \sum_{m\in K} V_m^1 \left(G_{km}^1 sen\left(\theta_{km}^1\right) - B_{km}^1 cos\left(\theta_{km}^1\right)\right) \tag{17}$$

where K denotes the buses directly connected to a given bus k including the bus k. B_{km}^1 e G_{km}^1 are the susceptance and conductance of a km branch for fundamental frequency ($h = 1$) and θ_{km}^1 is the angular difference between buses k and m.

Harmonic load flow is computed based on the application of Eq. (4), according to [25]. It represents the frequency domain response of the network subject to injected currents by harmonic sources (non-linear loads) modelled as constant current source. It also considers power system components models including generators, transmission lines, machines and loads in frequency domain.

As one of the main contributions of this research, this paper introduces power quality indices treated as inequality constraints that must be satisfied in order to find the optimal solution, which determines the maximum loadability, harmonic voltage magnitudes and angles. Critical buses related to voltage stability and harmonic distortion are determined based on Lagrange multipliers associated with the constraints of the proposed formulation.

2.2. Review of interior-point method

Due to the non linear nature associated to the optimisation problem, the solution will be provided by interior-point method, briefly described in this subsection according to references [26] and [27]. Traditionally, an optimisation problem can be formulated as presented by (18):

$$\begin{aligned} &\max f(\mathbf{x}) \\ &\textit{subject to:} \\ &\mathbf{g}(\mathbf{x}) = 0 \\ &\mathbf{h}(\mathbf{x}) \le 0 \end{aligned} \tag{18}$$

where $\mathbf{x}$ represents the variables vector, $f(\mathbf{x})$ is the objective function to be maximised, $\mathbf{g}(\mathbf{x})$ represents the equality constraints and $\mathbf{h}(\mathbf{x})$ the inequality constraints. The inequalities are transformed into equality constraints by introducing slack variables $\mathbf{s}$ as presented in (19). In this case, the barrier function parameter μ is added to the objective function to be maximised, in which n_{ineq} represent the number of inequality constraints of the problem.

$$\begin{aligned} &\max f(\mathbf{x}) - \mu \sum_{j=1}^{n_{ineq}} s_j \\ &\quad \textit{subject to:} \\ &\quad \mathbf{g}(\mathbf{x}) = 0 \\ &\mathbf{h}(\mathbf{x}) + \mathbf{s} = 0 \\ &\quad \mathbf{s} \ge 0 \end{aligned} \tag{19}$$

The Lagrangian function to be maximised is determined by Eq. (20), in which n_{eq} is the number of equality constraints.

$$L_{(\mathbf{x},\delta,\pi,\mu)} = f(\mathbf{x}) - \mu \sum_{j=1}^{n_{ineq}} s_j - \sum_{j=1}^{n_{eq}} \delta_j g_j(\mathbf{x}) - \sum_{j=1}^{n_{ineq}} \pi_j \left(h_j(\mathbf{x}) - s_j\right) \tag{20}$$

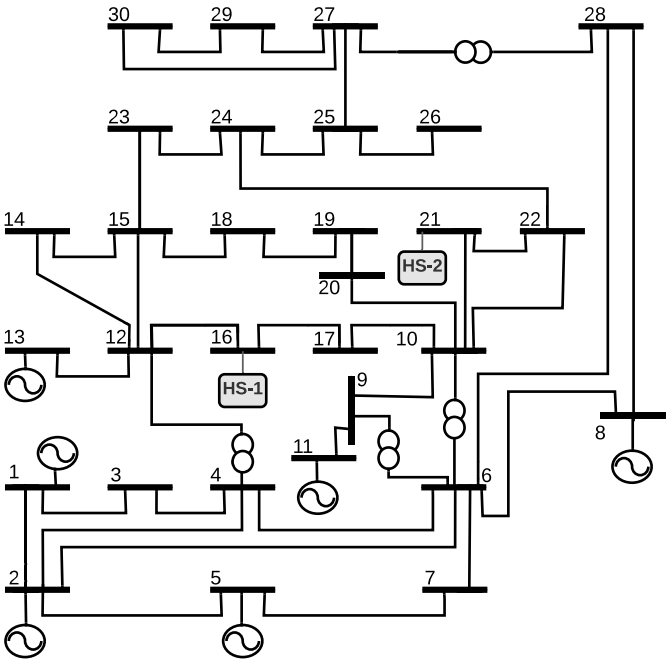

Fig. 1. IEEE 30-bus test system.

Table 1
Harmonic source (HS-1) data at bus 16.

h	I_k^h(%)	$\theta_k^{h,I}$ (°)
1	100.00	− 19.16
3	17.82	123.20
5	32.00	121.56
7	19.49	119.71

Based on the application of Karush-Kuhn-Tucker (KKT) first order optimality conditions, it is possible to calculate the derivatives of $L_{(\mathbf{x},\delta,\pi,\mu)}$ with respect to the state variables $\mathbf{x}$, and Lagrange multipliers associated with equality constraints δ_j and inequality constraints π_j, as presented in (21):

$$\frac{\partial L_{(x,\delta,\pi,\mu)}}{\partial x} = \frac{\partial L_{(x,\delta,\pi,\mu)}}{\partial \delta} = \frac{\partial L_{(x,\delta,\pi,\mu)}}{\partial \pi} = 0 \tag{21}$$

As the derivatives are set equal to zero, the response is calculated by Newton-Raphson iterative method as described by Hong and Gau [13].

It is important to notice that, at the local maximum ($\mathbf{x}^*$), active (binding) constraints, say $h(\mathbf{x}^*) = 0$, are associated with larger Lagrange multipliers which can be used to identify the inequalities which reach their corresponding limits. These inequalities have a major impact on the objective function value and may indicate critical areas when a constrained optimisation problem is formulated for analysing power systems operation according to [13] and [2].

The solution provided by interior point-method provides the Lagrange multipliers values according to Pillo and Roma [28], being their values useful to indicate the most critical buses once they are closely related to the system loadability according to Rodriguez-Garcia et al. [2] and Granville [26]. In this case, even if the global minimum or maximum is not guaranteed to be found, the KKT first order optimality conditions must be satisfied in order to find the optimal solution.

Note that larger Lagrange multipliers can be often associated with the most critical buses within the context of voltage stability assessment [2,27]. Additionally, it is known that, as load increases from a rated load factor ($\lambda = 1$) towards the maximum loadability, the Lagrange multipliers associated with maximum reactive power generation, have a decreasing behaviour as the power system approximates to the maximum loadability factor ($\lambda = \lambda_{\max}$) at the critical point.

3. The proposed Lagrange multipliers based indices

After the convergence of the optimisation problem, the maximum loadability margin and state variables are determined as well as the Lagrange multipliers of equality and inequality constraints.

Based on the Lagrange multipliers, it is possible to determine voltage stability indices responsible for indicating the proximity to the critical point. In this paper, three indices are proposed to identify critical areas of the network related to voltage stability, its corresponding total harmonic distortion and lack of reactive support, representing the main contribution of the paper.

The index presented in Eq. (22) is used for assessing the active constraint that reaches the corresponding minimum voltage magnitude. Similarly, the index presented in Eq. (23) is used for evaluating the inequality which reach the maximum THD value.

$$d_k^v = \frac{1}{1 + \left(\frac{\pi_k^v}{\lambda}\right)} \tag{22}$$

$$d_k^{thd} = \frac{1}{1 + \left(\frac{\pi_k^{thd}}{\lambda}\right)} \tag{23}$$

where π_k^v and π_k^{thd} are, respectively, the largest Lagrange multipliers associated with active constraints of voltage magnitudes and its total harmonic distortion.

Loadability factor λ is also considered to determine the index because Eqs. (22) and (23) tend to the unitary value as the power system approximates to the critical point, when all Lagrange multipliers are approximately equal to 0, as discussed in [2].

Indices d_k^v and d_k^{thd} are used in this paper to assess the largest Lagrange multipliers values associated with voltage magnitudes and voltage THD constraints, presented by inequalities (5) and (8) respectively. Their use enables the assessment of power quality deterioration for different scenarios, indicating the most sensitive buses related to undervoltages and their corresponding distortion limits.

It is expected that, when the system is voltage stable, these indices assume lower values. As the system approaches the critical point near the maximum loadability margin, they approach the unitary value serving as a relative measure of the proximity to the critical point.

Additionally, sensitivities relating reactive power injections to voltage magnitudes at each bus k can be used to identify critical buses of the network. The d_k^q index, presented by Eq. (24), is utilised for assessing voltage stability relating the largest Lagrange multipliers δ_k^q associated with reactive power equality constraints (3).

$$d_k^q = 1 - \frac{1}{1 + \left(\frac{\delta_k^q}{\lambda}\right)} \tag{24}$$

When the system is near to the critical point, d_k^q is calculated for each load bus with the objective of identifying which buses need additional reactive power support. The determination of the critical bus is compared with the traditional modal analysis in this paper in order to validate the results obtained using the proposed method.

4. Results and discussion

In order to prove the efficiency of the proposed method, simulations are carried out using IEEE 30-bus test system. Load and line data are presented in Appendix A, being the single line diagram of the power system presented in Fig. 1. Linear loads are assumed to be constant PQ model in the fundamental frequency. For other harmonic orders, they

Table 2
Harmonic source (HS-2) data at bus 21.

h	I_k^h(%)	$\theta_k^{h,I}$ (°)
1	100.00	− 19.68
3	4.52	120.90
5	5.67	116.17
7	2.75	110.92

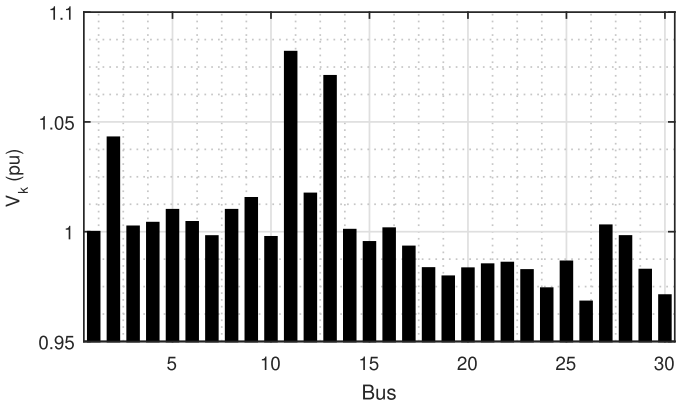

Fig. 2. Voltage magnitudes for the base case.

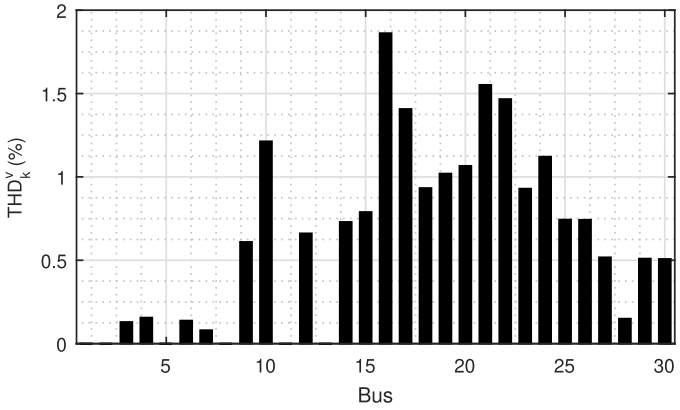

Fig. 3. Voltage THD for the base case.

Table 3
d_k^v behaviour for different case studies.

$V_k^{\min}$ (pu)	λ^* (pu)	π_k^v	d_k^v
0.95	1.1729	25.9015	0.0433
0.90	1.5898	21.0339	0.0703
0.80	2.1887	13.0299	0.1438
0.70	2.5543	7.6361	0.2507
0.60	2.7478	3.3456	0.4502
0.55	2.7909	1.4875	0.6523
0.52	2.8012	0.0464	0.9837

Table 4
d_k^q behaviour near the critical point ($\lambda = 2.8002$).

Bus	δ_k^q	d_k^q
30	351.4661	0.9921
29	42.4918	0.9382
26	33.5197	0.9229
24	18.8379	0.8706

Table 5
Comparative results with modal analysis.

Proposed method		Modal analysis	
Bus	Value	Bus	Value
30	0.9921	**30**	0.2647
29	0.9382	**29**	0.2110
26	0.9229	**26**	0.1019
24	0.8706	**24**	0.0950

are considered as parallel RL passive elements. The modelling of transmission lines, generators, loads and other elements is according to ran [25].

Non-linear loads are inserted into the network, being considered as current injection model determined by typical data of SVCs (Static Var Compensators) obtained from the case studies presented in [25]. The harmonic source spectrum of the non linear load at bus 16 is presented in Table 1 and the one which is localised at bus 21 is presented in Table 2.

The code was implemented using MATLAB software, using a computer Intel® Core™ i7-2600 CPU @ 3.40 GHz and 16 GB(RAM), with the operational system Windows-10. Interior-point method is implemented by the use of *fmincon* toolbox which handles non linear objective function and inequality constraints.

4.1. Load flow for the base case

In order to present the results for the base case, the harmonic load flow presented in reference [29] is used to determine the voltage magnitudes at 60Hz and their corresponding THD for all the system buses considering the system nominal load, as presented by Figs. 2 and 3, respectively.

It can be observed that, all the voltages are greater than 0.95 pu and THD values are all lower than 2%, indicating that the system is operating between acceptable limits considering power quality standards such as IEC 61000-3-2 and IEEE 519.

4.2. Determination of the proposed indices

Table 3 presents the results of the optimal loadability factor (λ^*) determined by the proposed formulation considering the lower bound of the voltage magnitudes decreasing from 0.95 pu (stable solutions) to the critical point. It is expected that, as the voltage magnitude lower bound is decreased, the maximum loadability is increased according to references [1,2,8].

Additionally, Lagrange multipliers π_k^v are shown for each case as well as the calculated by the Lagrange multiplier-based d_k^v index, as presented by Eq. (22). It can be noted that, as the system loadability factor increases, the d_k^v index tends to the unitary value, serving as a relative measure to the critical point.

In order to complete Table 3, upper bounds of the voltage magnitudes at system buses are equal to 1.10 pu. Voltage THD and IHD are set equal to 10%; current THD and IHD equal to 40%. The relaxation of these bounds allows the optimal loadability factor to be found limited only by the voltage magnitudes lower bounds, ensuring that there is no active (bidding) inequality constraint except the ones associated with undervoltages.

Once the system maximum loadability can be found by the proposed formulation, it is possible to calculate d_k^q associated the reactive power flow equality constraints based on their corresponding Lagrange multipliers δ_k^q,as shown by Eq. (24). As presented by Table 4, the index can be calculated for each load bus. The higher d_k^q index is, more critical the bus is considered within the context of voltage stability analysis. It means that this bus needs additional reactive power support.

These results show the applicability of the proposed method for identifying the critical buses related to lack of reactive support helping

Table 6
d_k^{thd} behaviour for different case studies.

THD_k^{max} (%)	λ^* (pu)	π_k^{thd}	d_k^{thd}
2.00	1.0781	1.6150	0.4003
3.00	1.6595	1.6562	0.5005
4.00	2.2301	1.4667	0.6032
5.00	2.7105	1.1064	0.7101
5.28	2.8012	0.0227	0.9920

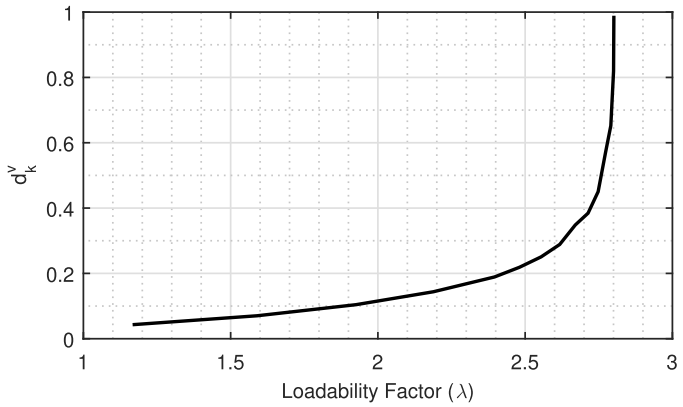

Fig. 4. d_k^v for different loadability factors.

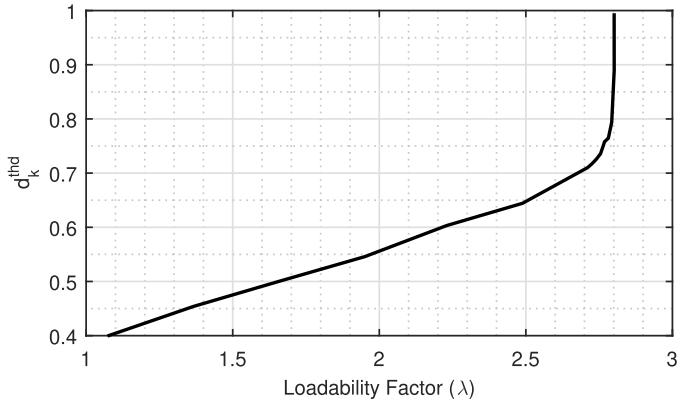

Fig. 5. d_k^{thd} for different loadability factors.

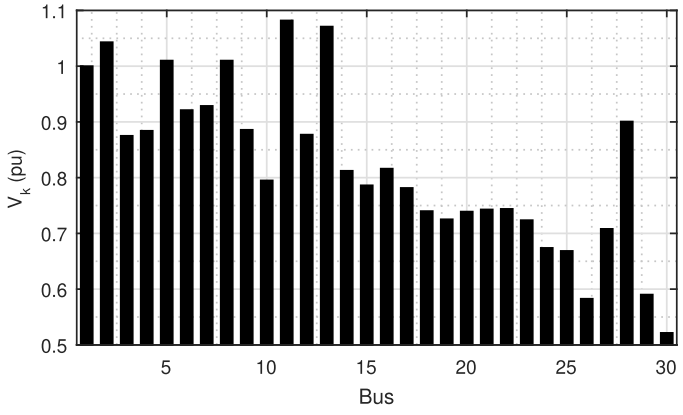

Fig. 6. Voltage magnitudes at the critical point.

operators to detect weakest buses due to voltage instability.

Table 5 presents a comparative evaluation considering the results found by the proposed method with modal analysis proposed by [11] which determines participation factors of the load buses to identify the weakest ones. It can be noted that the proposed methodology determines the same most critical buses of the system when compared to another method from the literature.

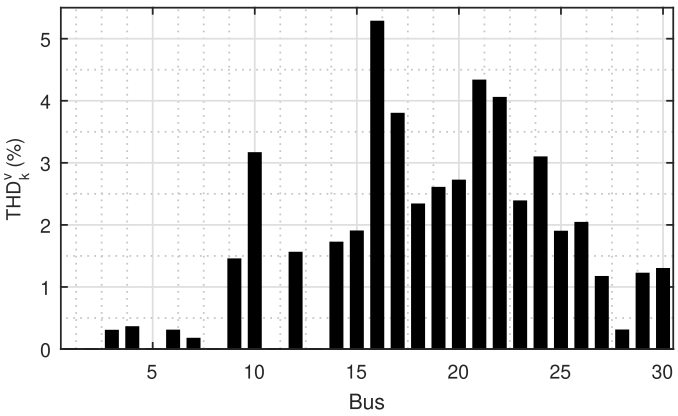

Fig. 7. Voltage THD at the critical point.

Table 7
d_k^v behaviour for different case studies with a contingency of the line 27–30.

V_k^{min} (pu)	λ^* (pu)	π_k^v	d_k^v
0.90	1.0790	14.6932	0.0684
0.80	1.5104	9.9132	0.1322
0.70	1.7872	5.7303	0.2374
0.60	1.9315	$7.66\ 10^{-8}$	1.0000

Table 6 presents the results of optimal loadability factor assuming that the active constraints are the ones associated with the voltage THD. According to the Eq. (24), the d_k^{thd} index value was quantified. In this case, lower bounds of voltage magnitudes are set equal to zero, as proposed by Rodriguez-Garcia et al. [2], in order to ensure that no active constraint is associated with voltage magnitude constraints. It is observed that the active constraints are always those related to voltage THD at bus 16 once this bus is associated with a large harmonic insertion into the system, contributing to its pollution and power quality degradation.

It can be noted from the results presented by Tables 3 and 6 that, as the system loadability increases, the proposed indices d_k^v and d_k^{thd} approach to the unitary value indicating the proximity to a critical point. In practice, these indices can be used in control centres to identify the weakest buses of the system related to voltage instability helping the operator to assess the phenomena of voltage stability and its harmonic distortion.

Fig. 4 presents the results for d_k^v index associated with the optimal loadability factor. Similarly, d_k^{thd} is calculated for each loadability factor determined by the proposed method, as presented in Fig. 5.

Note that, as the loadability factor increases towards the critical point, both indices approach the unitary value, serving as an indicator of the proximity of the system to an unstable point.

Figs. 6 and 7 present the results for voltage magnitudes and voltage THD for all the system buses at the critical point, respectively. Note that, in this case, voltage at bus 30 is 0.52 pu and THD is greater than 5% at bus 16. It serves to indicate that, at the critical point, not only the voltage magnitudes are exceeding acceptable limits imposed by standards but also their corresponding total harmonic distortion values.

4.2.1. Contingency analysis

In this case study, a contingency of the line connecting buses 27 and 30 is simulated in order to evaluate the impact on the maximum

Table 8
d_k^q behaviour near the critical point with a contingency of the line 27–30 (for $\lambda = 1.9057$).

Bus	δ_k^q	d_k^q
30	99.3003	0.9812
29	6.7778	0.7805
26	1.3563	0.4158
24	0.9017	0.3212

Table 9
d_k^{thd} behaviour for different case studies with a contingency of the line 27–30.

THD_k^{max} (%)	λ^* (pu)	π_k^{thd}	d_k^{thd}
2.00	1.0772	1.6091	0.4010
3.00	1.6540	1.6464	0.5012
3.50	1.9362	1.4811	0.5666
3.53	1.9512	1.2784	0.6042
3.54	1.9543	0.0044	0.9977

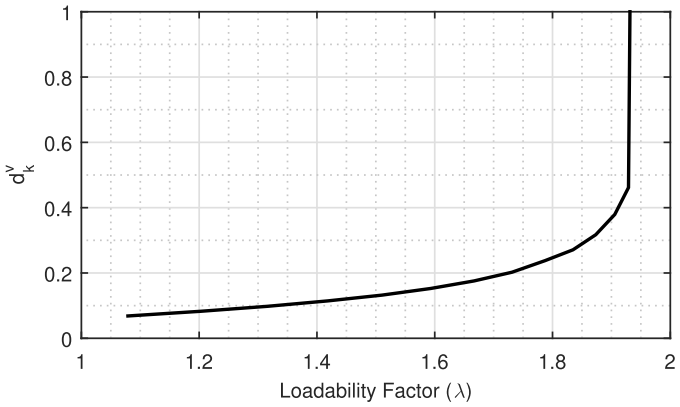

Fig. 8. d_k^v for different loadability factors with a contingency.

loadability margin determined by the proposed optimisation problem as well as the indices values in this situation.

Table 7 presents the values of d_k^v calculated for different cases decreasing the lower bounds of voltage magnitudes from stable solutions towards the critical point. Due to the line outage from the system, the maximum loadability margin is more restricted when compared to Table 3. The active constraints are always the ones associated with undervoltages at bus 30.

Table 8 presents the results of d_k^q near the critical point, indicating the most critical buses. In comparison to Table 4, Lagrange multipliers associated with the reactive power equations are smaller, indicating that, in this case, more reactive power support would be necessary to restore the system stability. This condition is expected since the line outage impact on the system operation.

The results for d_k^{thd} are presented in Table 9. The active constraints are associated with the voltage THD at bus 16, indicating this bus as a potential harmonic source for the system.

Figs. 8 and 9 present the behaviour of the indices d_k^v and d_k^{thd} for different loadability factors considering the contingency of the line 27–30. In this case, the behaviour of the indexes is more abrupt towards the critical point than the base case.

For this case, it can be concluded that bus 30 is related to lower values of undervoltages and the lack of reactive support and bus 16 is the bus that impact and degrade the most the power quality of the system due to large harmonic distortion values.

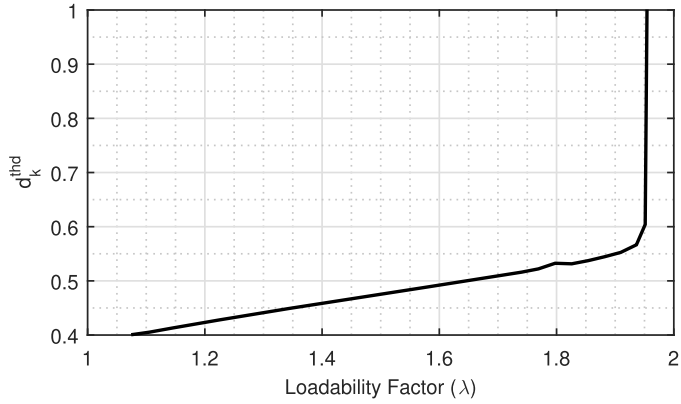

Fig. 9. d_k^{thd} for different loadability factors with a contingency.

4.2.2. *Dividing the 30-bus system into areas*

As presented by reference [13], the 30-bus system can be subdivided into the following areas:

- Area A composed of buses 1, 2, 4 5, 6, 7, 8 and 28;
- Area B including buses 9, 10, 11, 12, 13, 16 and 17;
- Area C composed of buses 14, 15, 18, 19, 20, 21 and 22;
- Area D including buses 23, 24, 25, 26, 29 and 30.

In this case study, the behaviour of the proposed indices will be evaluated considering the maximisation of the loadability factor for each area individually.

Instead of maximising the loadability for all the system buses, only the buses within the area C will be considered.

Area C is chosen once there is a non linear load at bus 21, while the other non linear load is within area B. Table 10 presents the results for d_k^v for different conditions. Since only one single area is progressively increasing the power demand, the maximum loadability is larger than the other cases. In this case study, the active constraint related to voltage magnitude lower bound is the bus 19.

Table 11 presents the results of d_k^q index, indicating the most weakest buses in this case. It is interesting to notice that, once the system load is only increased for area C, the most critical buses are different from the other case studies but they are correctly identified by the proposed method.

Table 12 presents the results for index d_k^{thd} for the active constraints related to voltage THD. In this case, the bus 21 which is within area C is

Table 10
d_k^v behaviour for different case studies with increment of load of area C.

V_k^{min} (pu)	λ^* (pu)	π_k^v	d_k^v
0.95	1.5632	8.5271	0.1549
0.90	2.4437	7.4715	0.2465
0.80	3.7882	5.0828	0.4270
0.70	4.6598	3.0720	0.6027
0.60	5.1337	1.3680	0.7896
0.56	5.2255	0.5337	0.9073
0.52	5.2694	0.0334	0.9937

Table 11
d_k^q behaviour near the critical point with increment of load on area C (for $\lambda = 5.2255$).

Bus	δ_k^q	d_k^q
19	826.1773	0.9937
21	547.1900	0.9905
18	198.6817	0.9744
15	195.8009	0.9740

Table 12
d_k^{thd} behaviour for different case studies with increment of load on area C.

THD_k^{max} (%)	λ^* (pu)	π_k^{thd}	d_k^{thd}
2.00	1.4875	1.6321	0.5120
3.00	2.5156	0.4970	0.8350
4.00	3.5567	0.4645	0.8845
5.00	4.4488	0.2051	0.9559
6.00	5.0502	0.1693	0.9676
6.50	5.2120	0.1056	0.9801
6.92	5.2693	0.0168	0.9968

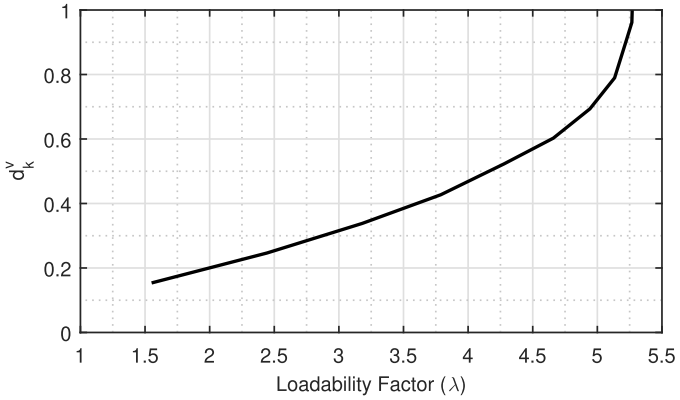

Fig. 10. d_k^v for different loadability factors with increment of load of area C.

related to the active constraint. Note that, in this case, once the system load is only increased in one area, the voltage THD assumes values extremely larger than the other cases (approximately 7%). It consists on an important analysis to be made. As described in [25], the non linear loads inject harmonic currents into the system and they are absorbed by the linear loads of the other buses, modelled as RL passive elements. Once the system load is only increased in a single area, the attenuation of the producing harmonic currents for the other load buses is more restrictive which may justify their larger values.

Figs. 10 and 11 present the behaviour of the indices d_k^v and d_k^{thd} for different loadability factors considering the increment of load only in area C. Differently from the other cases, the active constraints associated with the calculation of d_k^v and d_k^{thd} are the buses 19 and 21, respectively. In this case, it can be concluded that bus 19 is associated with extreme values of undervoltages and bus 21 would be the bus which mostly impact and deteriorate the power quality of the system due to large harmonic distortion values.

In Fig. 11, a different behaviour is associated with the d_k^{thd} index. For maximum allowed voltage THD values from 2% to 3%, the active constraints are related to bus 16. However, as the maximum allowable value

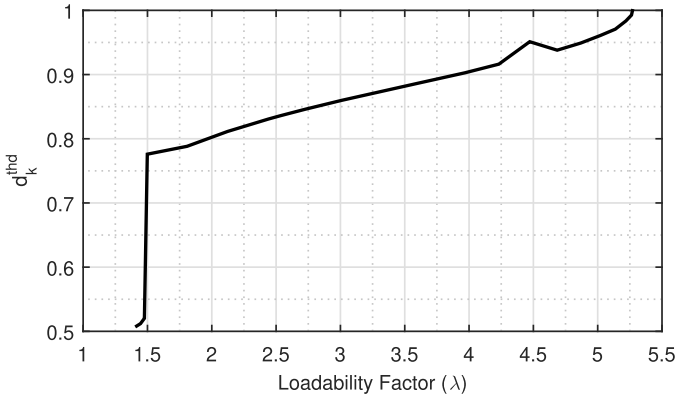

Fig. 11. d_k^{thd} for different loadability factors with increment of load of area C.

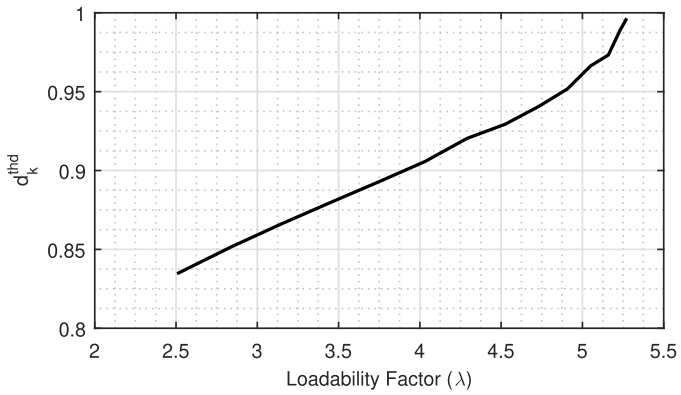

Fig. 12. d_k^{thd} for different loadability factors with increment of load of area C (for THD_k^v from 3% to 6.92%).

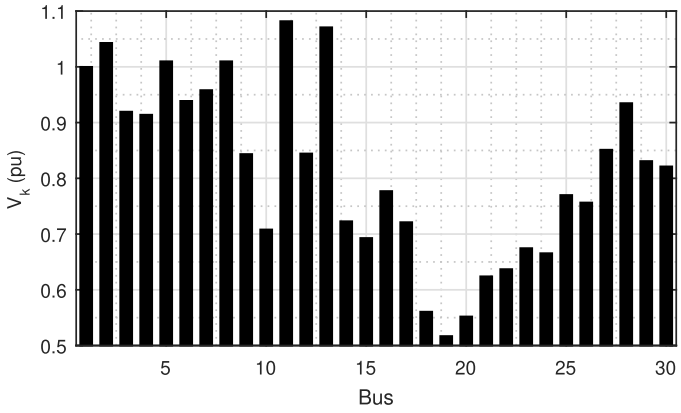

Fig. 13. Voltage magnitudes with increment of load of area C.

increases from 3% to the critical case, the active constraints are associated with bus 21. In order to emphasise the results for THD_k^v from 3% to 6.92%, Fig. 12 present the behaviour of the index within these limits.

Voltage magnitudes and voltage THD are presented in Figs. 13 and 14, respectively, at the critical point. As expected voltage THD is larger at bus 21 due to the load increase only in area C.

4.2.3. *Case study with additional harmonic sources*

In this case study, other non linear loads are added to the 30-bus test system in order to consider the impact of more harmonic sources in the network and also to test the application of the proposed indices in a different scenario. For the computational simulations, harmonic currents are injected at buses 3, 14 and 30 being their magnitudes values

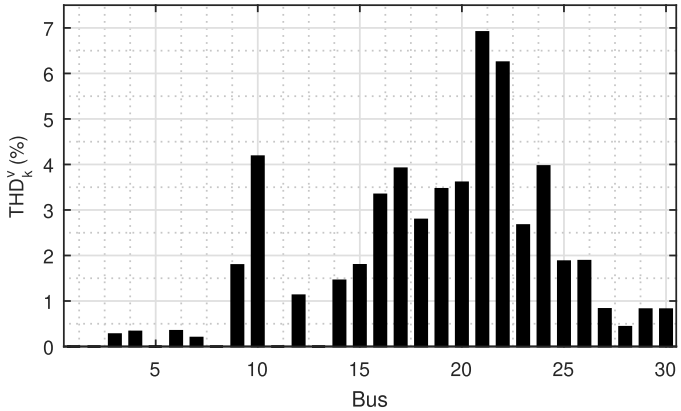

Fig. 14. Voltage THD with increment of load of area C.

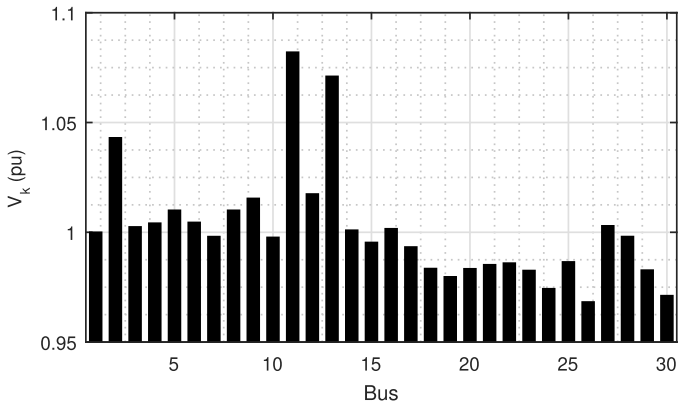

Fig. 15. Voltage magnitudes for additional harmonic sources.

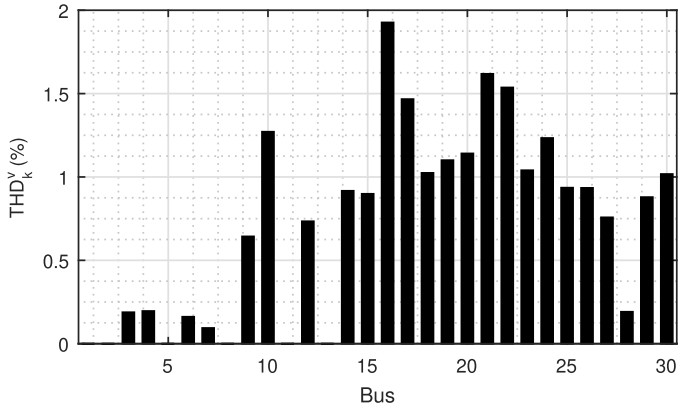

Fig. 16. Voltage THD for additional harmonic sources.

Table 13
d_k^v behaviour for different case studies with additional harmonic sources.

V_k^{min} (pu)	λ^* (pu)	π_k^v	d_k^v
0.90	1.5898	21.0257	0.0703
0.80	2.1887	13.0329	0.1438
0.70	2.5543	7.6345	0.2507
0.60	2.7478	3.3540	0.4503
0.55	2.7909	1.4861	0.6525
0.52	2.8012	0.0463	0.9838

equal to 10% of the harmonic spectrum presented in Table 1.

Considering the test system under nominal load, Figs. 15 and 16 present the voltage magnitudes at 60Hz and their corresponding THD for all the system buses. The main impact of the introduction of more harmonic sources is on the voltage THD, which is higher than the base case.

Analogously to the other case studies, Table 13 presents the values of d_k^v calculated for different scenarios, being the active constraints associated with undervoltages at bus 30. As the loadability factor increases, the greatest Lagrange multiplier approaches zero and the proposed index tends to assume an unitary value.

Table 14 presents the results of d_k^q near the critical point indicating buses 30, 29, 26 and 24 as the critical ones. Note that the same buses are indicated in Table 5 when compared to the traditional modal analysis.

The results for d_k^{thd} are presented in Table 15 being the active constraints associated with the voltage THD at bus 16. Compared to the base case, d_k^{thd} assumes a higher value due to the introduction of more harmonic currents injected into the system at buses 3, 14 and 30. Note that the indices have a similar behaviour to the base case, proving its efficiency and viability.

Table 14
d_k^q behaviour near the critical point with additional harmonic sources (for $\lambda = 2.8002$).

Bus	δ_k^q	d_k^q
30	353.1793	0.9921
29	42.7040	0.9385
26	33.6921	0.9233
24	18.9185	0.8711

Table 15
d_k^{thd} behaviour for different case studies with additional harmonic sources.

THD_k^{max} (%)	λ^* (pu)	π_k^{thd}	d_k^{thd}
2.00	1.0400	1.5691	0.3986
3.00	1.6081	1.6265	0.4972
4.00	2.1736	1.5219	0.5882
5.04	2.6789	1.1482	0.7000
5.26	2.7631	0.9323	0.7477
5.40	2.8016	0.0788	0.9726

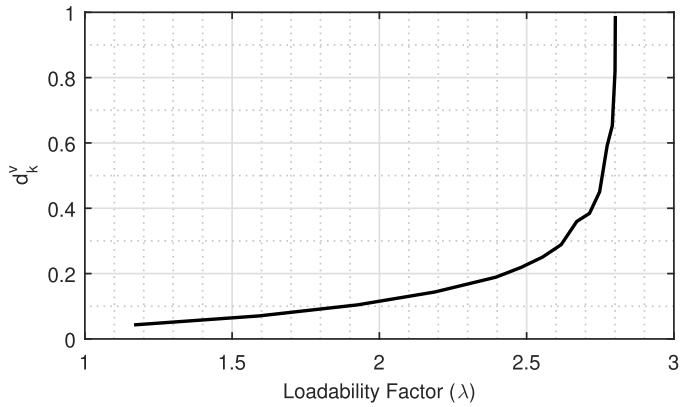

Fig. 17. d_k^v for different loadability factors with additional harmonic sources.

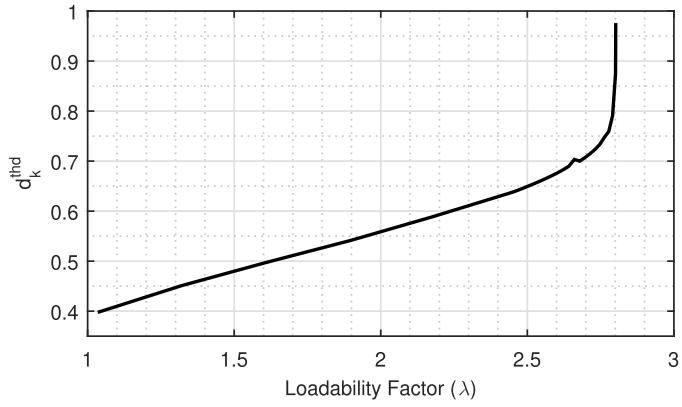

Fig. 18. d_k^{thd} for different loadability factors with additional harmonic sources.

Figs. 17 and 18 present the behaviour of the indices d_k^v and d_k^{thd} for different loadability factors, respectively.

Figs. 19 and 20 present the voltage magnitudes and their corresponding THD for all the system buses at the critical point.

Based on the results obtained in this case study, it is possible to note that, although more harmonic sources are introduced into the system, the proposed indices presented a satisfactory performance being validated for different scenarios.

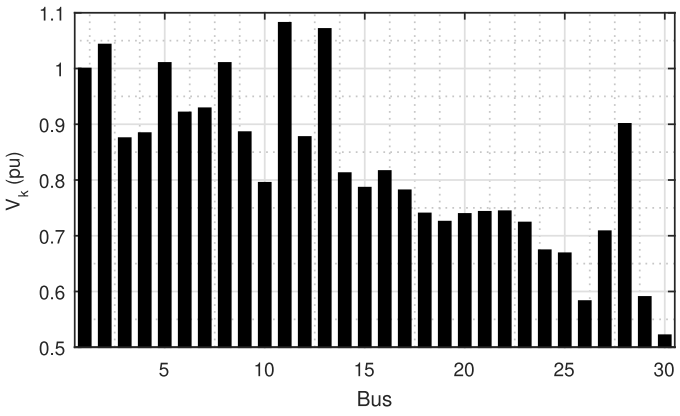

Fig. 19. Voltage magnitudes at the critical point with additional harmonic sources.

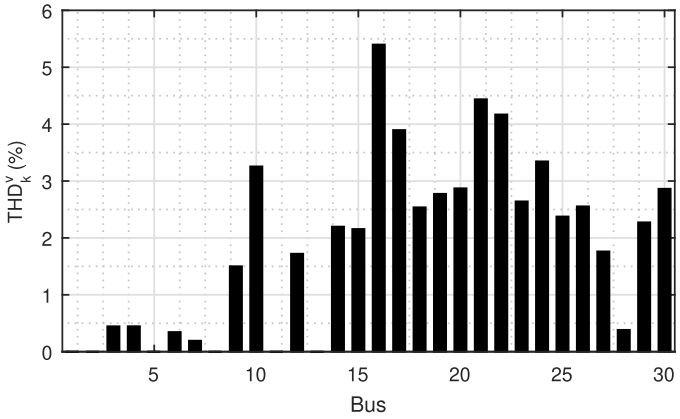

Fig. 20. Voltage THD at the critical point with additional harmonic sources.

5. Conclusions

This paper presented a novel optimisation model for harmonic distortion and voltage stability assessment. An objective function is determined for maximising the system loadability considering inequality constraints related to power flow equations, voltage magnitudes and harmonic distortion. The solution is provided by interior point method in which Lagrange multipliers are used to determine new indices d_k^v, d_k^{thd} and d_k^q for assessing active constraints related to undervoltages, voltage THD and reactive power support.

By the presented results, it can be concluded that the proposed method is able to indicate the proximity to a critical point within the context of voltage stability assessment due to the fact of indices d_k^v and d_k^{thd} approach to the unitary value as the system loading increases towards the critical point. Additionally, the active constraints are associated with the most sensitive buses of the system related to undervoltages and voltage THD.

These indices can be used for real time applications to serve as an indicator of the proximity to a voltage collapse. It may help operators to proceed with caution when the system is near to a critical point, taking the proper actions to restore the system stability.

The proposed indices are determined based on the optimal calculated values of voltage magnitudes and their THD since these values are often referred to as important power quality indicators in standards with restrictive limits.

Another useful feature is the proposed d_k^q index which can identify the most critical buses of the system due to lack of reactive power support. By a comparison with the traditional modal analysis, the same buses are identified as the weakest ones validating the methodology. Additionally, it would be useful to identify the buses in which future reinforcement can be considered to maintain the system operating under normal conditions such as the allocation of capacitor banks, static var compensators or synchronous condensers.

Future works include the evaluation of larger systems, the impact of the installation of capacitor banks, background distortion and the possibility to use the method for other applications within the context of power quality assessment such as resonance detection.

In this research paper, the proposed indices were developed and evaluated for transmission systems. The application of the proposed method in distribution networks can also be investigated in future works.

CRediT authorship contribution statement

Mariana O.N. Teixeira: Conceptualization, Methodology, Data curation, Writing – original draft. **Igor D. Melo:** Visualization, Investigation, Supervision, Writing – original draft. **João A.P. Filho:** Writing – review & editing.

Declaration of Competing Interest

The authors declare that they have no known competing financial interests or personal relationships that could have appeared to influence the work reported in this paper.

Acknowledgment

This study was financed in part by the Coordenação de Aperfeiçoamento de Pessoal de Nível Superior - Brasil (CAPES) - Finance Code 001. The authors would also like to thank UFJF (Universidade Federal de Juiz de Fora) and PPEE (Programa de Ps Graduação em Engenharia Elétrica).

Appendix A. 30-bus test system data

Nominal load and line data of the 30-bus system are presented in Table A.16 and A.17, respectively, according to reference [30]. The active/reactive powers generation limits associated with each generator capacity is according to the original reference [30].

Table A1
Load data.

k	type	V_k (pu)	θ_k (rad)	$P_{g,k}$ (MW)	$Q_{g,k}$ (Mvar)	$P_{l,k}$ (MW)	$Q_{l,k}$ (Mvar)
1	$V\theta$	1.000	0.0	260.20	− 16.1	-	-
2	PV	1.043	0.0	40.00	50.00	21.70	12.70
3	PQ	1.000	0.0	-	-	2.40	1.20
4	PQ	1.000	0.0	-	-	7.60	1.60
5	PV	1.010	0.0	0.00	37.00	94.20	19.0
6	PQ	1.000	0.0	-	-	0.00	0.00
7	PQ	1.000	0.0	-	-	22.80	10.90
8	PV	1.010	0.0	0.00	37.30	30.00	30.00
9	PQ	1.000	0.0	-	-	0.00	0.00
10	PQ	1.000	0.0	-	-	5.80	2.00
11	PV	1.082	0.0	0.00	16.20	0.00	0.00
12	PQ	1.000	0.0	-	-	11.20	7.50
13	PV	1.071	0.0	0.00	10.60	0.00	0.00
14	PQ	1.000	0.0	-	-	6.20	1.60
15	PQ	1.000	0.0	-	-	8.20	2.50
16	PQ	1.000	0.0	-	-	3.50	1.80
17	PQ	1.000	0.0	-	-	9.00	5.80
18	PQ	1.000	0.0	-	-	3.20	0.90

(*continued on next page*)

Table A1 (*continued*)

k	type	V_k (pu)	θ_k (rad)	$P_{g,k}$ (MW)	$Q_{g,k}$ (Mvar)	$P_{l,k}$ (MW)	$Q_{l,k}$ (Mvar)
19	*PQ*	1.000	0.0	-	-	9.50	3.40
20	*PQ*	1.000	0.0	-	-	2.20	0.70
21	*PQ*	1.000	0.0	-	-	17.50	11.2
22	*PQ*	1.000	0.0	-	-	0.00	0.00
23	*PQ*	1.000	0.0	-	-	3.20	1.60
24	*PQ*	1.000	0.0	-	-	8.70	6.70
25	*PQ*	1.000	0.0	-	-	0.00	0.00
26	*PQ*	1.000	0.0	-	-	3.50	2.30
27	*PQ*	1.000	0.0	-	-	0.00	0.00
28	*PQ*	1.000	0.0	-	-	0.00	0.00
29	*PQ*	1.000	0.0	-	-	2.40	0.90
30	*PQ*	1.000	0.0	-	-	10.50	1.90

Table A2
Line data.

from	to	r (Ω)	x (Ω)	y (Ω^{-1})	tap
1	2	0.0192	0.0575	0.0528	-
1	3	0.0452	0.1852	0.0408	-
2	4	0.0570	0.1737	0.0368	-
3	4	0.0132	0.0379	0.0084	-
2	5	0.0472	0.1983	0.0418	-
2	6	0.0581	0.1763	0.0374	-
4	6	0.0119	0.0414	0.0090	-
5	7	0.0460	0.1160	0.0204	-
6	7	0.0267	0.0820	0.0170	-
6	8	0.0120	0.0420	0.0090	-
6	9	0.0100	0.2080	-	1.015
6	10	0.0100	0.5560	-	0.963
9	11	0.0000	0.2080	-	-
9	10	0.0000	0.1100	-	-
4	12	0.0100	0.2560	-	1.013
12	13	0.0000	0.1400	-	-
12	14	0.1231	0.2559	-	-
12	15	0.0662	0.3104	-	-
12	16	0.0945	0.1987	-	-
14	15	0.2210	0.1997	-	-
16	17	0.0824	0.1932	-	-
15	18	0.1070	0.2185	-	-
18	19	0.0639	0.1292	-	-
19	20	0.0340	0.0680	-	-
10	20	0.0936	0.2090	-	-
10	17	0.0324	0.0845	-	-
10	21	0.0348	0.0749	-	-
10	22	0.0727	0.1499	-	-
21	22	0.0116	0.0236	-	-
15	23	0.1000	0.2020	-	-
22	24	0.1550	0.1790	-	-
23	24	0.1320	0.2700	-	-
24	25	0.1895	0.3292	-	-
25	26	0.2544	0.3800	-	-
25	27	0.1093	0.2087	-	-
28	27	0.0100	0.3690	-	-
27	29	0.2198	0.4153	-	-
27	30	0.3202	0.6027	-	-
29	30	0.2399	0.4533	-	-
8	28	0.0636	0.2000	-	-
6	28	0.0169	0.0599	-	-

Linear loads are assumed to be constant PQ model in the fundamental frequency. For other harmonic orders, they are considered as parallel RL passive elements. The modelling of transmission lines, generators, loads and other elements is according to [25].

References

[1] P.A. Aghdam, H. Khoshkhoo, Voltage stability assessment algorithm to predict power system loadability margin, IET Generation, Transmission & Distribution (2020).
[2] L. Rodriguez-Garcia, S. Perez-Londono, J. Mora-Florez, An optimization-based approach for load modelling dependent voltage stability analysis, Electric Power Systems Research 177 (2019) 105960.
[3] I.D. de Melo, J.L.R. Pereira, C.A. Duque, M.P. Antunes, L.R.M. Silva, M.A. de Souza, Power quality monitoring using synchronized phasor measurements: An approach based on hardware-in-the-loop simulations. 2019 IEEE Milan PowerTech, IEEE, 2019, pp. 1–6.
[4] M. Tian, Y. Wang, J. Li, Comprehensive harmonic responsibility calculation based on different weighting methods, Energies 12 (23) (2019) 4449.
[5] S. Bhattacharyya, S. Cobben, P. Ribeiro, W. Kling, Harmonic emission limits and responsibilities at a point of connection, IET generation, transmission & distribution 6 (3) (2012) 256–264.
[6] P. Kundur, N.J. Balu, M.G. Lauby, Power system stability and control volume 7, McGraw-hill New York, 1994.
[7] Y. Song, D.J. Hill, T. Liu, State-in-mode analysis of the power flow jacobian for static voltage stability, International Journal of Electrical Power & Energy Systems 105 (2019) 671–678.
[8] V. Ajjarapu, C. Christy, The continuation power flow: a tool for steady state voltage stability analysis, IEEE transactions on Power Systems 7 (1) (1992) 416–423.
[9] T.J. Overbye, I. Dobson, C.L. DeMarco, Qv curve interpretations of energy measures for voltage security, IEEE Transactions on Power Systems 9 (1) (1994) 331–340.
[10] A.K. Sharma, A. Saxena, R. Tiwari, Voltage stability assessment using gvsm and preventive control using svc, International Journal of Computer Applications 142 (11) (2016) 23–31.
[11] B. Gao, G. Morison, P. Kundur, Voltage stability evaluation using modal analysis, IEEE transactions on power systems 7 (4) (1992) 1529–1542.
[12] R. Salgado, A. Zeitune, Critical solutions of maximum loadability via direct methods, Journal of Control, Automation and Electrical Systems 24 (3) (2013) 349–360.
[13] Y.-Y. Hong, C.-H. Gau, Voltage stability indicator for identification of the weakest bus/area in power systems, IEE Proceedings-Generation, Transmission and Distribution 141 (4) (1994) 305–309.
[14] J. Modarresi, E. Gholipour, A. Khodabakhshian, A comprehensive review of the voltage stability indices, Renewable and Sustainable Energy Reviews 63 (2016) 1–12.
[15] E.G. Amador, A. Llamas, J.C.M. Maldonado, J.C.R. Caro, J.E.V. Resendiz, Pmu based voltage stability indices with intermediate load compensation, IEEE Latin America Transactions 16 (4) (2018) 1172–1179.
[16] S. Dasgupta, M. Paramasivam, U. Vaidya, V. Ajjarapu, Real-time monitoring of short-term voltage stability using pmu data, IEEE Transactions on Power Systems 28 (4) (2013) 3702–3711.
[17] S. Polster, H. Renner, D.T. Duong, K. Uhlen, Voltage stability monitoring using a modified thevenin impedance. 2017 IEEE Manchester PowerTech, IEEE, 2017, pp. 1–6.
[18] J.N. da Costa, J.A. Passos Filho, R.M. Henriques, Loading margin sensitivity analysis in systems with significant wind power generation penetration, Electric Power Systems Research 175 (2019) 105900.
[19] A.F.M. Nor, M. Sulaiman, A.F.A. Kadir, R. Omar, Determining voltage stability margin values by measuring the hypotenuse under pv and qv curves, International Journal of Electrical Engineering and Applied Sciences (IJEEAS) 1 (1) (2018) 25–30.
[20] X. Xu, Z. Yan, M. Shahidehpour, H. Wang, S. Chen, Power system voltage stability evaluation considering renewable energy with correlated variabilities, IEEE Transactions on Power Systems 33 (3) (2017) 3236–3245.
[21] L.S. Neves, L.F.C. Alberto, H.-D. Chiang, A fast method for detecting limit-induced bifurcation in electric power systems, Electric Power Systems Research 180 (2020) 106101.
[22] IEEE Recommended Practice and Requirements for Harmonic Control in Electric Power Systems, Standard, IEEE, 2014.
[23] IEEE Draft Recommended Practice for Monitoring Electric Power Quality, Standard, IEEE, 2014.
[24] Electromagnetic compatibility (EMC) Part 3-14, Standard, IEC, 2012.
[25] Tutorial on Harmonics Modeling and Simulation, IEEE Power Energy Society (PES), 2003.
[26] S. Granville, Optimal reactive dispatch through interior point methods, IEEE Transactions on power systems 9 (1) (1994) 136–146.
[27] L.A. Ferreira, A.Z. de Souza, S. Granville, J.M. Lima, Interior point method applied to voltage collapse problems and system-losses-reduction, IEE Proceedings-Generation, Transmission and Distribution 149 (2) (2002) 165–170.
[28] G. Pillo, M. Roma, Large-scale nonlinear optimization volume 83, Springer Science & Business Media, 2006.
[29] A. Variz, J. Pereira, S. Carneiro Jr, P. Barbosa, Three-phase harmonic power flow using the current injection method. IEEE International Conference on Harmonics and Power Quality, 2006.
[30] A.R. Al-Roomi, Power Flow Test Systems Repository, 2015, https://al-roomi.org/power-flow.